TRENDS IN SCIENCES 2026; 23(2): 11528
https://doi.org/10.48048/tis.2026.11528 RESEARCH ARTICLE

Aquilaria Crassna Pierre Ex Lecomte Leaf Extract Induces Apoptosis and Immunogenic Cell Death in Breast Cancer Cells, Enhancing Anti-Tumor Effects of Dendritic Cells

Pinyada Pho-on[1], Sangkab Sudsaward[1], Piriya Luangwattananun[2,3], Aussara Panya[4], Chutamas Thepmalee[5], Mutita Junking[2,3], Eakkaluk Wongwad[6,7], Kornkanok Ingkaninan[6], Pattareeya Sereesantiwong[8], Warintorn Wongho[1], Pa-thai Yenchitsomanas[2,3] and Sasiprapa Khunchai[1,*]

[1]*Department of Anatomy, Faculty of Medical Science, Naresuan University, Phitsanulok 65000, Thailand*
[2]*Siriraj Center of Research Excellence for Cancer Immunotherapy (SiCORE-CIT), Faculty of Medicine, Siriraj Hospital, Mahidol University, Bangkok 10700, Thailand*
[3]*Division of Molecular Medicine, Research Department, Faculty of Medicine Siriraj Hospital, Mahidol University, Bangkok 10700, Thailand*
[4]*Cell Engineering for Cancer Therapy Research Group, Department of Biology, Faculty of Science, Chiang Mai University, Chiang Mai 50200, Thailand*
[5]*Division of Biochemistry, School of Medical Sciences, University of Phayao, Phayao 56000, Thailand*
[6]*Centre of Excellence in Cannabis Research, Faculty of Pharmaceutical Sciences and Center of Excellence for Innovation in Chemistry, Naresuan University, Phitsanulok 65000, Thailand*
[7]*Department of Cosmetic Sciences, School of Pharmaceutical Sciences, University of Phayao, Phayao 56000, Thailand*
[8]*Department of Doctor of Optometry, Faculty of Allied Health Sciences, Naresuan University, Phitsanulok 65000, Thailand*

([*]Corresponding author's e-mail: Sasiprapak@nu.ac.th)

Received: 7 August 2025, Revised: 22 August 2025, Accepted: 1 September 2025, Published: 1 November 2025

Abstract

Aquilaria crassna (A. crassna) Pierre ex Lecomte, commonly known as agarwood, is traditionally used in medicinal preparations. Previous studies suggest anti-cancer properties in *A. crassna* leaf extract but the mechanisms and its involvement in immunogenic cell death (ICD) remain unexplored. This study investigates the impact of *A. crassna* Pierre ex Lecomte leaf extract (AE) on anti-cancer activity, specifically inducing ICD in triple-negative breast cancer (TNBC), and enhancing dendritic cell (DC) anti-tumor effects. *A. crassna* water extract underwent HPLC analysis. TNBC cells (MDA-MB-231) and non-tumorigenic epithelial cell lines, fibrocystic disease, (MCF-10A) were treated with different concentrations of AE for cytotoxicity testing by MTT assay. To assess ICD induction, danger-associated molecular patterns (DAMPs) including ectoCRT, secreted ATP, and HMGB1 were measured through staining, ATP bioluminescence, immunoblotting, and ELISA, respectively. AE-treated cells and DAMP-containing supernatants were administered to monocyte-derived DCs, evaluating impact on DC immunophenotype, maturation, and phagocytosis via flow cytometry. HPLC analysis identified AE compounds: iriflophenone 3,5-C-β-D-diglucoside, iriflophenone 3-C-β-D-glucoside, mangiferin, and genkwanin 5-O-β-primevoside (concentrations: 4.80, 1.04, 4.54 and 0.18 %w/w). MDA-MB-231 treated with AE exhibited ICD induction, evident in increased ectoCRT, secreted ATP, and HMGB1 levels. DCs exposed to AE-treated cells and DAMP-containing supernatant displayed enhanced phagocytic activity and maturation, with elevated CD86, CD80, CD83, and HLA-DR expression. In conclusion, AE exhibits immunomodulatory potential by inducing ICD in TNBC, suggesting therapeutic applications for its anti-cancer effects and a promising role in cancer immunotherapy.

Keywords: *Aquilaria crassna* Pierre ex Lecompte leaf extract, Immunogenic cell death, Dendritic cell maturation/activation, Triple-negative breast cancer, Cancer immunotherapy

Introduction

Aquilaria plants, belonging to the Thymelaeaceae family, are a highly valued botanical species native to Southeast Asia. Among these, *A. crassna* Pierre ex Lecomte, also known as Krisana in Thai, holds significant cultural and medicinal importance. Traditionally, *A. crassna* has been employed in the production of perfumes, incense, and various medicinal purposes. Its applications span a wide range of health conditions including infectious and inflammatory diseases, arthritis, cardiac disorders, digestive disorders, neurodegenerative disorders and sedative disorders [1-3]. The heartwood of *A. crassna* is an essential component of the traditional Thai remedy 'Ya-hom', which is employed to support treatments for aging, cardiovascular disorders, and inflammation [4]. Additionally, leaves of *A. crassna,* exhibit a diverse range of beneficial properties such as anti-aging, antioxidant, anti-inflammatory, anti-bacteria, neuroprotective, and vasorelaxant activities [1,5-7]. The leaves are used in herbal teas, as well as being included in herbal soups, instant noodles, and biscuits [8,9].

In recent years, there has been a growing interest in investigating the potential anti-cancer properties of *Aquilaria* species, with particular focus on *A. crassna*. A study conducted by Hashim *et al.* [8] highlighted the anti-cancer effects of agarwood essential oils obtained from Malaysian market. The research underscored the oils' efficacy in diminishing the viability of breast cancer cells and impeding their attachment. Moreover, the essential oil derived from *A. crassna* demonstrated substantial anti-proliferative activity against various cancer types, including pancreatic, colorectal, prostatic adenocarcinoma, and breast cancer cells, while also demonstrating anti-metastatic properties specifically in pancreatic cancer cells [10,11]. Consistently, *A. crassna* extract has been shown to induce apoptosis in breast cancer cells by upregulating caspase-3 and downregulating the expression of BCl-2 and proliferating cell nuclear antigen (PCNA) [12]. While previous research has demonstrated the ability of *A. crassna* to induce cancer cell death, there are currently no studies reporting its potential involvement in immunogenic cell death (ICD).

ICD is a regulated form of cell death that triggers the immune system's anti-tumor response by generating neoantigens and the release of specific danger-associated molecule patterns (DAMPs). DAMPs, including surface calreticulin (CRT) or ectoCRT, adenosine triphosphate (ATP), and high mobility group box-1 protein (HMGB-1), are expressed and secreted by dying cancer cells, playing a crucial role in activating antigen-presenting cells (APCs) and facilitating T-cell infiltration [13,14]. The interaction between ectoCRT and CD91 receptors, as well as ATP and P2X7 receptors, serve as "eat me" and "find me" signals, respectively, enabling the recognition of cancer cells by APCs such as dendritic cells (DCs), macrophages, and monocytes. Additionally, the binding between HMGB1 and TLR-4 receptors promotes DC maturation, which subsequently activates CD8+ T cells and/or CD4+ T cells, leading to the elimination of residual cancer cells with resistance [13,15,16]. Consequently, inducing ICD in tumors holds promising potential for immunotherapeutic approaches, as it can trigger an immune response and enhance the anti-tumor activity of immune cells to eliminate the surviving tumor cells.

Interestingly, mangiferin (1,3,6,7-terahydroxyxanthone-C2-b-D-glucoside), a bioactive compound found in *A. crassna,* has been previously reported for anti-cancer properties and immunostimulatory effect [17,18]. However, no studies have investigated the involvement of mangiferin or AE in modulating ICD. Therefore, the objective of this study was to elucidate the ability of AE to induce ICD in MDA-MB-231 cells, a triple-negative breast cancer (TNBC) cell line. We established that AE treatment induces ICD in cancer cells, substantiated by alterations in the expression levels of ectoCRT, ATP, and HMGB1. Furthermore, we explored the effects of culture cells and supernatant derived from AE-treated MDA-MB-231 cells, rich in DAMPs, on the maturation and function of dendritic cells (DCs). These findings contribute valuable insights into the potential immunotherapeutic application of *A. crassna*.

Materials and methods

Cell culture

The human triple-negative breast cancer (TNBC) cell line, MDA-MB-231, was procured from ATCC-LGC (#HTB-26; Middlesex, UK). A non-tumorigenic epithelial cell lines, fibrocystic disease, (MCF-10A) was

obtained from ATCC (Manassas, VA, USA). Cultivation of the cells was carried out in Dulbecco's Modified Eagle's Medium (DMEM) (Gibco, Thermo Fisher Scientific, Waltham, MA, USA) supplement with 10% fetal bovine serum (FBS) (Gibco, Thermo Fisher Scientific, Waltham, MA, USA), 100 μnits/mL penicillin, and 100 mg/mL streptomycin. Incubation was maintained at 37 °C with 5% CO_2 under humidified conditions.

Plant materials, extraction preparation, and high-performance liquid chromatography (HPLC) analysis

The aqueous extract derived from the leaves of *A. crassna* Pierre ex Lecomte (AE) was meticulously prepared and quantified by our research team member (EW) using a protocol consistent with prior descriptions [7,19]. In summary, young leaves (from tops 1 to 3) were subjected to cleaning, followed by drying at 100 °C for 3 h in a hot-air oven and subsequently grinding into powder. The resulting leaf powder (500 g) underwent infusion in 5 L of hot water at temperatures ranging from 95 - 100 °C for 30 min. The supernatant was then filtered, freeze-dried, and stored at –20 °C for future use.

Analysis of the 4 major bioactive compounds previously identified and reported - compound 1 (3,5-*C*-*β*-D-diglucoside), compound 2 (3-*C*-*β*-D-glucoside), and compound 3 (mangiferin), and compound 4 (genkwanin 5-*O*-*β*-primevoside) - was conducted using an HPLC system from Shimadzu Corporation (Shimadzu; Kyoto, Japan), featuring a separation module (Shimadzu LC-20A) and a detector (Shimadzu SPD-20A UV/Vis). A validated HPLC method, consistent with a previous report was employed for quantification [7]. Compounds 1, 2, and 4 were isolated as reference standards according to a prior report, while compound 3 was generously provided by our colleague (Assist. Prof. Dr. Uthai Wichai of the Faculty of Science, Naresuan University, Thailand) [7]. Linearities for each standard were determined using calibration curves plotted between the peak area and concentration of mixed solutions of compounds 1 - 3 (concentration ranged from 4.0 - 64.0 μg/mL) and compound 4 (concentration ranged from 0.5 - 8.0 μg/mL).

Cytotoxic assays

The cytotoxic impact of AE on the viability of MDA-MB-231 and MCF-10A cells was assessed using the [3-(4,5-dimethylthiazol-2-yl)-2,5-diphenyltetrazolium 24 bromide] or MTT assay. Cells (10^4 cells/well) were initially seeded in a 96-well plate for 24 h, followed by exposure to varying concentrations of AE (0 - 640 μg/mL) for 24 h and 48 h. Subsequently, 0.5 mg/mL of MTT reagent (Sigma Aldrich, St. Louis, MO, USA) was introduced, and the cells were further incubated for 2 h. After removal of the supernatant, dimethyl sulfoxide (DMSO) was employed to dissolve formazan crystals, yielding a purple solution. The optimal density (OD) at 575 nm was measured to assess the reducing capacity of living cells, with OD 690 nm serving as a reference. The percentage of cell viability was calculated relative to the untreated condition (0 μg/mL), set as 100%.

To elucidate the potential role of AE in the induction of ICD, an apoptotic assay was conducted. MDA-MB-231 cells treated with AE, under the same conditions as the MTT assay, were harvested, washed with phosphate buffer saline (PBS), and stained with AnnexinV and 7-AAD dyes at room temperature for 20 min. The Muse™ Cell Analyzer (Merck Millipore, Burlington, MA, USA) was then employed, following the manufacturer's instruction, to analyze apoptotic cell death. The percentage of apoptosis cells, including early apoptosis, late apoptosis, and total apoptosis was calculated through software analysis of the Muse™ Cell Analyzer.

Cell surface staining and flow cytometry

The impact of AE on ectoCRT expression was investigated using flow cytometry. MDA-MB-231 cells were initially seeded at 2.5×10^5 cells in a 6-well plate for 24 h before exposure to various concentrations of AE, mirroring those mentioned earlier. Following 6 and 12 h of the treatment, cells were subjected to staining with anti-CRT antibody (Abcam, Cambridge, UK) for 1 h, succeeded by incubation with Alexa488®-conjugated secondary antibody (Invitrogen, Thermo Fisher Scientific, Waltham, MA, USA) for an additional hour. EctoCRT-stained cells were promptly post-stained with AnnexinV and propidium iodide (PI) (ImmunoTools, Aidenbach, Germany) and analyzed using a BD Accuri C6 Flow Cytometer. Data were then processed through

BD flow analysis software (BD Biosciences, San Joes, CA, USA). Total apoptotic cells were gated, and the analysis focused on ectoCRT-positive signals. EctoCRT expression data were presented as the percentage of positive cells and relative mean fluorescence intensity (MFI).

ATP bioluminescent assay

The ATP secreted from cells treated with AE into the extracellular compartment was quantified using an ATP bioluminescent assay (Roche, Basel, Switzerland). MDA-MB-231 cells were seeded at 5×10^4 cells in a 24-well plate one day before treatment with AE (0 - 640 µg/mL) for 24 and 48 h. Conditioned media were harvested and subjected to centrifugation at 8,000 rpm for 1 min to eliminate cellular debris. Twenty-five µL of conditioned media was combined with 25 µL of luciferin, thoroughly mixed, and then analyzed for ATP content as luciferase light units using the Luminometer Lumat LB 9507 (Berthold Technologies, Bad Wildbad, Germany). ATP concentrations were determined from an ATP calibration curve following the manufacturer's instructions.

Immunoblotting assay and enzyme-linked immunosorbent assay (ELISA)

The induction of HMGB1 by AE in both the intracellular and extracellular compartments was assessed through immunoblotting and enzyme-linked immunosorbent assay (ELISA), respectively. MDA-MB-231 cells (2×10^5 cells) were seeded into 6-well plate and treated with AE under the same conditions as described earlier. Total proteins were extracted from the cells and utilized for immunoblotting, employing a primary antibody specific to HMGB1 (Abcam, Cambridge, UK) and β-actin (Cell signaling, Danvers, MA, USA) at a 1:1000. Protein detection was accomplished using anti-rabbit-HRP- and anti-mouse-HRP-conjugated secondary antibodies (Invitrogen, Thermo Fisher Scientific, Waltham, MA, USA), respectively. Clarity™ western ECL substrate (BioRad, Hercules, CA, USA) served as the detection reagent, and protein bands were visualized on an X-ray film via a film developer.

For the evaluation of extracellular HMGB1, conditioned media from MDA-MB 231 cells treated with AE at concentrations of 160 and 320 µg/mL for 48 h were analyzed using a human HMGB-1/HMG-1 ELISA kit (Novus Biologicals, Littleton, CO, USA). This assay quantified the level of secreted HMGB1, and concentrations were determined in accordance with the manufacturer's protocol.

Peripheral blood mononuclear cells and immature dendritic cells preparation

The experimental protocols involving human blood samples received approval from the Naresuan University Institutional Review Board (NUIRB No. P1-0155/2564). Peripheral blood mononuclear cells (PBMCs) were sourced from healthy volunteer donors who provided informed consent by signing consent forms prior to participating in the experiments. In brief, PBMCs were isolated from whole blood using Ficoll-Hypaque Gradient Centrifugation (Millipore Corporation, Burlington, MA, USA) and cultured in AIM-V media (Gibco, Thermo Fisher Scientific, Waltham, MA, USA) in a 12-well plate (1×10^7 cells) for 2 h to allow for the adherence of cells, particularly monocytes, the precursor cells. Monocyte-derived DCs were generated by introducing a final concentration of 50 ng/mL of granulocyte-macrophage colony stimulating factor (GM-CSF) and 25 ng/mL of interleukin-4 (IL-4) (ImmunoTools, Aidenbach, Germany) to the adherent monocytes, followed by a 5-day incubation period. The resulting monocyte-derived DCs were characterized as immature dendritic cells (iDCs).

Phagocytotic assay

The study investigated the capacity of AE to trigger ICD and enhance the phagocytotic activity of iDCs through a phagocytotic assay. MDA-MB-231 cells, genetically modified to consistently express red fluorescent protein (RFP), underwent treatment with AE at concentrations of 0, 160 and 320 µg/mL for 48 h to induce ICD. For the phagocytosis assay, the iDCs were pre-stained with CellTracker™ Green CMFDA dye (Invitrogen, Thermo Fisher Scientific, Waltham, MA, USA) at a concentration of 10 µM in plain RPMI for 15 min. resulting in the generation of green fluorescent DCs. Pre-stained iDCs were subsequently washed twice with plain RPMI and exposed to both culture cells and conditioned media from the respective treatments. Following a 4-h pulsing period, the pulsed iDCs were

examined for double-positive signals. This involved initially gating for green fluorescent-positive iDCs and subsequently analyzing for RFP-positive signals using a flow cytometer and previously described analysis software. The data was presented as the number of double-positive cells, indicating the engulfment of cancer cells by DCs or DC phagocytosis.

Morphological observation and immunophenotyping

The maturation and activation of iDCs pulsed with AE-induced ICD were validated through an examination of morphological and phenotypic characteristics. MDA-MB-231 cells, initially seeded into a 100 mm^2 dish (2.5×10^6 cells) for 24 h were subjected to AE treatment under conditions previously established for AE-induced ICD. The cells underwent lysis through 3 cycles of freezing and thawing: Immersion in liquid nitrogen for 1.5 min followed by a 5-min. incubation in a 37 °C water bath. The resulting lysates were collected as cell lysate, while conditioned media were collected, concentrated to a final 20× concentration through Amicon® ultra 2 centrifugations (Merck Millipore, Burlington, MA, USA), and stored as conditioned media. The prepared iDCs were then pulsed under various conditions: plain AIM-V medium for control iDCs, AIM-V medium supplemented with interferon-gamma (IFN-γ) at 50 ng/mL and tumor necrosis factor-alpha (TNF-α) at 50 ng/mL for positive control of DC maturation, or AIM-V medium plus 100 µg of cell lysates and 500 µg of concentrated conditioned media from untreated condition (iDCs +medium) or treated conditions (iDCs + AE 160 µg/mL and iDCs + AE 320 µg/mL), respectively. After a 2-day pulsing period, morphological maturation of the pulsed iDCs was assessed by observation under a light microscope at a 20x magnification. For phenotypic maturation/activation evaluation, pulsed iDCs underwent immunophenotyping using specific fluorescent-conjugated monoclonal antibodies targeting a DC marker (CD11c-APC) and co-stimulatory molecules, including CD40-FITC, HLA-DR-FITC, (ImmunoTools, Aidenbach, Germany) CD80-PE, CD83-PE, and CD86-PE (eBioscience, Thermo Fisher Scientific, San Diego, CA, USA). Isotype control antibodies (eBioscience, Thermo Fisher Scientific, San Diego, CA, USA) corresponding to each primary antibody were used as controls in all experiments. Immunophenotyping was carried out and analyzed using a flow cytometer and the previously described analysis software.

Statistical analysis

The result was demonstrated as the mean ± standard error of the mean (Mean ± SEM). All statistical analysis was derived from a minimum of 3 independent biological experiments. GraphPad Prism version 8.4.3 (GraphPad Software, Inc., San Diego, CA, USA) was employed to assess significant differences in means, utilizing Student's unpaired t-test for comparisons between 2 groups and 1-way analysis of variance (ANOVA) with Dunnett's test for comparisons among multiple groups. A threshold of $p < 0.05$ was applied to determine statistical significance.

Results and discussion

HPLC chromatographic profiling and quantification of bioactive components in AE

To ascertain the bioactive constituents within the AE extract, we employed high-performance liquid chromatography (HPLC) for the comprehensive characterization and quantification of individual compound concentrations. Starting with 500 g of leaf powder, our process yielded a dried AE with a weight/weight (%w/w) of 24.82. Our examination unveiled the presence of all 4 primary bioactive compounds, namely iriflophenone 3,5-*C*-*β*-D-diglucoside (compound 1), iriflophenone 3-*C*-*β*-D-glucoside (compound 2), mangiferin (compound 3), and genkwanin 5-*O*-*β*-primevoside (compound 4). The quantification of compounds 1 - 4 revealed the following concentrations: Compound 1, 4.80 ± 0.09 %w/w; compound 2, 1.04 ± 0.01 %w/w; compound 3, 4.54 ± 0.33 %w/w; and compound 4, 0.18 ± 0.02 %w/w. Notably, compounds 1 and 3 emerged as the most abundant constituents in AE. Additionally, the linearity assessment for each standard, derived from the calibration curve encompassing all compounds, yielded r^2 values ≥ 0.995, affirming the appropriateness of this HPLC method for determining compounds 1 - 4 [7]. **Figures 1(a)** - **1(c)** depict the chromatographic HPLC profile of these compounds along with their respective chemical structures. The concentration data, expressed as %w/w, are presented in **Table 1** for reference.

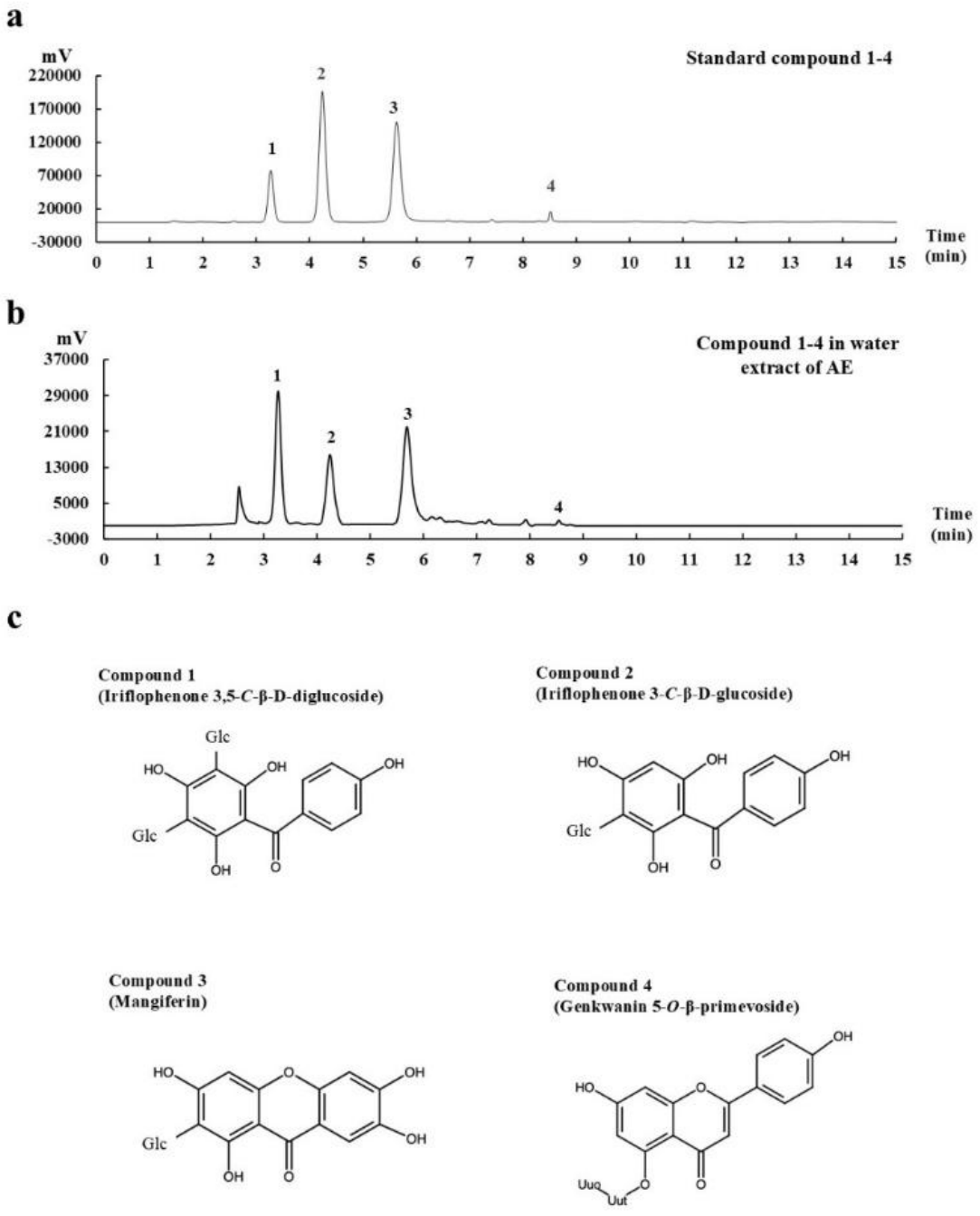

Figure 1 High-performance liquid chromatography (HPLC) profiling of water extract of AE. The chemical profile of the water extract of AE was analyzed using HPLC. A reference standard mixture, comprising 64 µg/mL of compound 1 (Iriflophenone 3,5-*C*-*β*-D-diglucoside), compound 2 (Iriflophenone 3-*C*-*β*-D-glucoside), compound 3 (Mangiferin), and 8 µg/mL of compound 4 (Genkwanin 5-*O*-*β*-primevoside), served as a reference (a). Chromatograms exhibit the identified peak of compounds 1 - 4 in the water extract of AE prepared at a concentration of 200 µg/mL, compared to the standard reference (b). Chemical structures of compounds 1 - 4 are presented (c).

Table 1 Concentrations of compounds 1 - 4 in water extract of AE. The dried AE, derived from 500 g of leaf powder, constituted 24.82 %w/w. Quantification of compounds 1 - 4 was achieved through HPLC analysis, utilizing a reference standard curve. The results are expressed as a percentage of weight/weight (%w/w) as detailed in **Table 1**.

Compound no.	Compound name	Concentration of compound (%w/w)
1	Iriflophenone 3,5-c-β-D-diglucoside	4.80 ± 0.09
2	Iriflophenone 3-C-β-D-glucoside	1.04 ± 0.01
3	Mangiferin	4.54 ± 0.33
4	Genkwanin 5-O-β-primevoside	0.18 ± 0.02

Cytotoxic effect and apoptotic induction of AE

The initial crucial step in assessing the potential of any agent as an ICD inducer involves evaluating its cytotoxic effects on target cells. In this context, we conducted an in-depth examination of the cytotoxicity of AE on MDA-MB-231 cells (TNBC) and MCF-10A (non-tumorigenic epithelial cells). To achieve this, we employed the MTT assay, treating MDA-MB-231 cells and MCF-10A cells with varying concentrations of AE (ranging from 0 to 640 µg/mL) for 24 and 48 h. Our findings revealed a notable cytotoxic impact of AE on MDA-MB-231 cells, characterized by a dose-dependent reduction in cell viability compared to untreated condition (0 µg/mL), as illustrated in **Figure 2(a)**. The most substantial declines in cell viability were observed at concentrations of 160 - 640 µg/mL after 24 h (62.50 ± 9.00%, 32.40 ± 10.70% and 14.70 ± 4.30%, respectively) and at concentrations of 80 - 640 µg/mL after 48 h (57.70 ± 4.90%, 42.90 ± 9.80%, 21.70 ± 7.20% and 9.90 ± 3.60%, respectively). The half-maximal inhibitory concentration (IC_{50}) of AE was determined to be 148.3 µg/mL after 24 h and 91.93 µg/mL after 48 h. Meanwhile AE did not show the remarkable harmfulness on non-tumorigenic cells, MCF10A, as observed in TNBC although the significant reduced cell viability was revealed at concentrations 10 - 640 µg/mL after 24 h (94.97 ± 0.00%, 95.10 ± 0.78%, 85.03 ± 0.42%, 89.40 ± 0.74%, 85.50 ± 0.59%, 81.66 ± 0.34%, and 84.78 ± 0.31%, respectively) and at concentrations of 40 - 640 µg/mL after 48 h (78.12 ± 2.70%, 77.71 ± 2.72%, 76.73 ± 3.68%, 71.83 ± 3.17%, and 73.84 ± 1.07%, respectively, (**Figure 2(b)**). These results underscore the specific significant cytotoxic potential of AE on TNBC (MDA-MB-231 cells), particularly at higher concentrations and longer exposure durations, providing valuable insights into its potential as an ICD inducer.

Beyond evaluating cytotoxicity, it is essential to assess the induction of regulated cell death, specifically apoptosis. Our investigation into the apoptotic potential of AE involved treating MDA-MB-231 cells under the same conditions as in the MTT assays. Following 24 and 48 h of treatment, cells were stained with AnnexinV and 7-AAD dyes, and subsequent analysis was conducted using Muse™ Cell Analyzer, as detailed previously. Our results demonstrated that AE induced apoptosis in MDA-MB-231 cells in a dose-dependent manner at both 24 h (**Figures 2(C)** and **2(d)**) and 48 h (**Figures 2(e)** and **2(f)**). Significant inductions of apoptosis were noted at concentrations ranging from 40 to 640 µg/mL at both time points. The average percentages of total apoptotic cells, encompassing both early and late apoptosis, were 19.93 ± 1.00%, 25.69 ± 0.90%, 26.39 ± 1.80%, 30.66 ± 4.50%, 42.19 ± 5.30% at 24 h, and 23.25 ± 4.60%, 24.47 ± 2.90%, 27.42 ± 5.30%, 32.07 ± 3.10%, and 61.77 ± 3.00% at 48 h, respectively. Collectively, our findings substantiate the conclusion that AE induces a cytotoxic effect on TNBC cells, with one of the underlying mechanisms involving the induction of apoptosis.

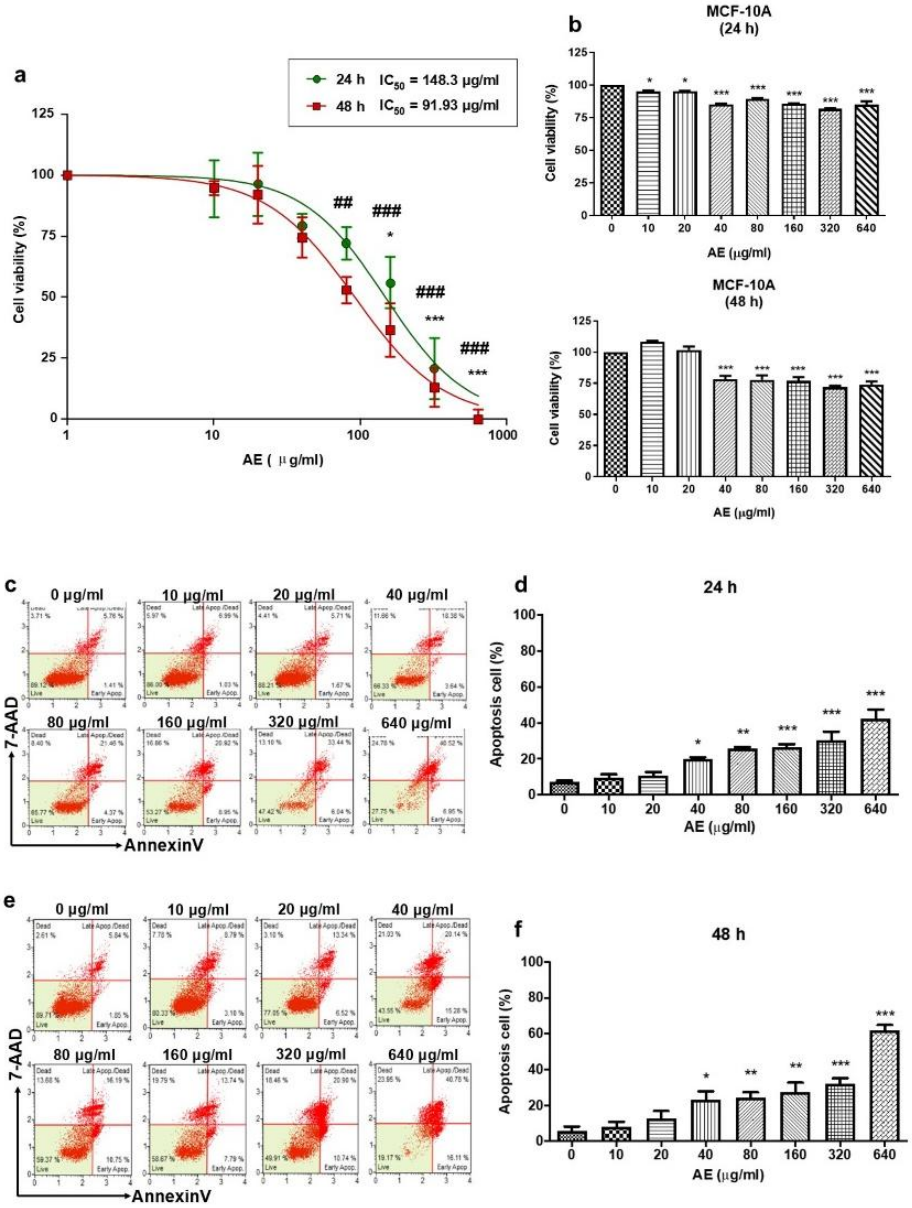

Figure 2 Cytotoxic effects of AE on MDA-MB-231 and MCF-10A cells as evidenced by MTT and apoptotic assays. MDA-MB-231 (a) and MCF-10A cells (b) were exposed to AE concentrations ranging from 0 to 640 µg/mL for 24 and 48 h. Cell viability percentages were assessed using the MTT assay. Representative histograms from Annexin V/7AAD staining in MDA-MB-231 cells, analyzed by Muse™ Cell Analyzer illustrate cell populations categorized as live (Annexin $V^-/7AAD^-$), early apoptotic (Annexin $V^+/7AAD^-$), late apoptotic (Annexin $V^+/7AAD^+$), dead cells (Annexin $V^-/7AAD^+$) at 24 h (c) and 48 h (e). Bar graphs depict the percentages of total apoptotic cells at 24 h (d) and 48 h (f). The mean ± SEM of at least 3-independent experiments is represented. The statistical analysis was investigated using differences in means compared to the untreated group (0 µg/mL). * and *** denote $p < 0.05$ and < 0.001 at 24 h while $^{###}$ indicates $p < 0.001$ at 48 h, respectively.

Expression of 3 hallmarks of DAMPs induced by AE

As the realm of ICD, the manifestation of DAMPs in distressed or dying cancer cells stands as a pivotal indicator. Our investigation honed in on 3 extensively studied DAMPs: ectoCRT, secreted ATP, and secreted HMGB1. Notably, apoptosis, a principal form of regulated cell death (RCD), is intricately linked with ICD [13]. Our study specifically delved into the expression of ectoCRT, the surface form of CRT, to gauge CRT translocation to the plasma membrane. Initially, we gated the apoptotic population in MDA-

MB-231 cells subjected to varying concentrations of AE for 6 and 12 h (**Figure 3(a)**). A substantial upswing in ectoCRT expression was discerned at 320 µg/mL after 12 h of treatment, with a relative mean fluorescence intensity (MFI) of 3.59 ± 0.4, contrasting with the untreated control (0 µg/mL) at 1.92 ± 0.2. Although other concentrations and the percentages of ectoCRT-positive cells exhibited an ascending trend (**Figures 3(f)** and **3(g)**), statistical significance for AE was not achieved after 6 h of the treatment (**Figures 3(c)** and **3(d)**).

To fortify the claim of AE as a robust ICD inducer, we scrutinized the levels of secreted ATP and HMGB1 in the extracellular milieu. The ATP bioluminescent assay illuminated a significant surge in secreted ATP in AE-treated MDA-MB-231 cells at concentrations of 160 and 320 µg/mL, compared to the untreated control at 24 h (0.40 ± 0.02 and 1.18 ± 0.24 nM, respectively) and 48 h (2.09 ± 0.67 and 3.40 ± 1.18 nM, respectively) (**Figure 3(h)**). Further affirming the potential ICD-inducing impact of AE, both intracellular and extracellular HMGB1 levels were examined at 48 h. Immunoblotting showcased a remarkable escalation in normalized intracellular HMGB1 at 320 µg/mL relative to the untreated control (1.47 ± 0.27 and 0.53 ± 0.16, respectively) (**Figures 3(i)** and **3(j)**). Consistent findings were corroborated for extracellular HMGB1 levels via ELISA, demonstrating a significant increase at 320 µg/mL of AE treatment compared to the untreated control (59.72 ± 19.65 and 3.37 ± 1.29 ng/mL, respectively) (**Figure 3(k)**).

Collectively, our results underscore that AE serves as an inducer of ICD, substantiated by the elevation in expression of all 3 of DAMPs hallmarks: ectoCRT, ATP, and HMGB1. Based on these outcomes, we denoted the conditions with AE treatment at concentrations of 160 and 320 µg/mL for 48 h as "AE-induced ICD" or "DAMPs-expressing conditions" in our study.

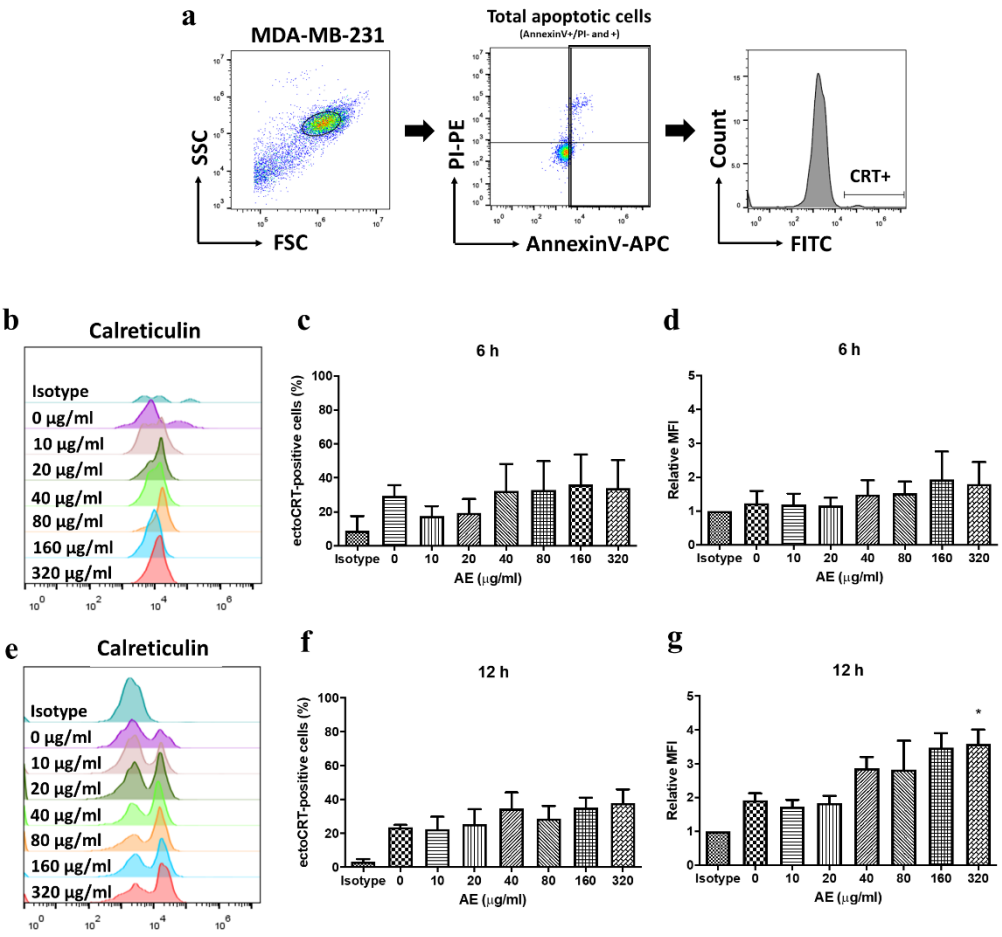

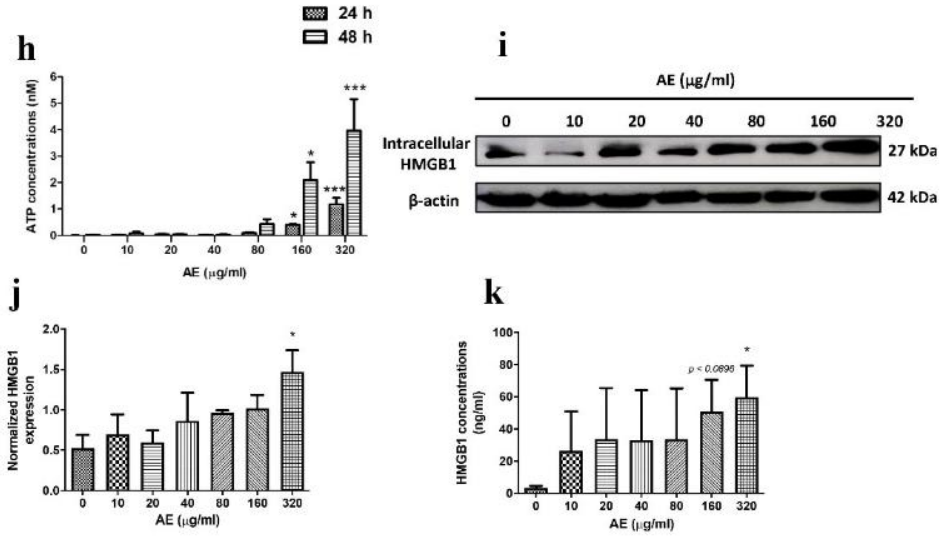

Figure 3 Expression of 3 hallmarks of DAMPs induced by AE in apoptotic cells. MDA-MB-231 cells were treated with AE at concentrations ranging from 0 to 320 μg/mL. At 6 and 12 h, cells were stained for ectoCRT expression using an anti-CRT antibody, followed by apoptotic staining with Annexin V/PI dyes. Gating strategies were employed for the selection of total apoptotic cells (a). Representative histograms, percentages of ectoCRT-positive cells, and the relative mean fluorescence or MFI of ectoCRT expression at 6 h (b-d) and 12 h (e-g) were analyzed by flow cytometry, respectively. The bar graph depicts the mean ± SEM of at least 3 independent experiments. * indicates $p < 0.05$. The conditioned media were assessed for secreted ATP using an ATP bioluminescent assay at 24 h and 48 h (h). Simultaneously, total intracellular HMGB1 expression was analyzed by immunoblotting at 48 h, with a representative result shown in (i). The band intensity, normalized with β-actin, was compared to the control (0 μg/mL) (j). The concentrations of secreted HMGB1 in conditioned media at 48 h were determined by ELISA and calculated relative to standard curve following the manufacturer's protocol (k). Data represents mean ± SEM of at least 3 independent experiments. * indicates $p < 0.05$, and *** indicates $p < 0.001$.

Phagocytotic activity of iDCs pulsed with AE-induced ICD

In light of ICD elevating the immunogenicity of tumor, especially in terms of their recognition by antigen-presenting cells (APCs) like dendritic cells (DCs), it was imperative to assess the phagocytotic activity of DCs exposed to AE-induced ICD conditions (160 and 320 μg/mL after 48 h of AE treatment). Immature DCs (iDCs) were incubated with AE-induced ICD for 4 h and subsequently examined for phagocytotic activity. This was achieved by scrutinizing double-positive signals from green fluorescent- labeled DCs and red fluorescent protein (RFP)-expressing MDA-MB-231 cells using both flow cytometry and immunofluorescence staining. Representative images from a fluorescence microscope revealed a distinctive merged orange signal emanating from green fluorescent- labeled DCs and RFP-expressing MDA-MB-231 cells in iDcs pulsed with AE-induced ICD at 320 μg/mL (**Figure 4(b)**).

Consistent results were obtained through flow cytometry analysis. The DC cell population (green fluorescence-positive cells; **Figure 4(c)** in iDCs pulsed with AE-induced ICD conditions at 160 and 320 μg/mL displayed an augmentation in the percentage of double-positive staining cells (green fluorescent- labeled DCs and RFP-expressing MDA-MB-231 cells) at 6.70 ± 2.14% and 12.57 ± 4.61%, respectively, in comparison to non-pulsed conditions (DCs pulsed with medium; 2.49 ± 0.78%) as depicted in **Figure 4(d)**. These findings strongly suggest that AE-induced ICD heightens the phagocytosis ability of DC in engulfing breast cancer (BC) cells.

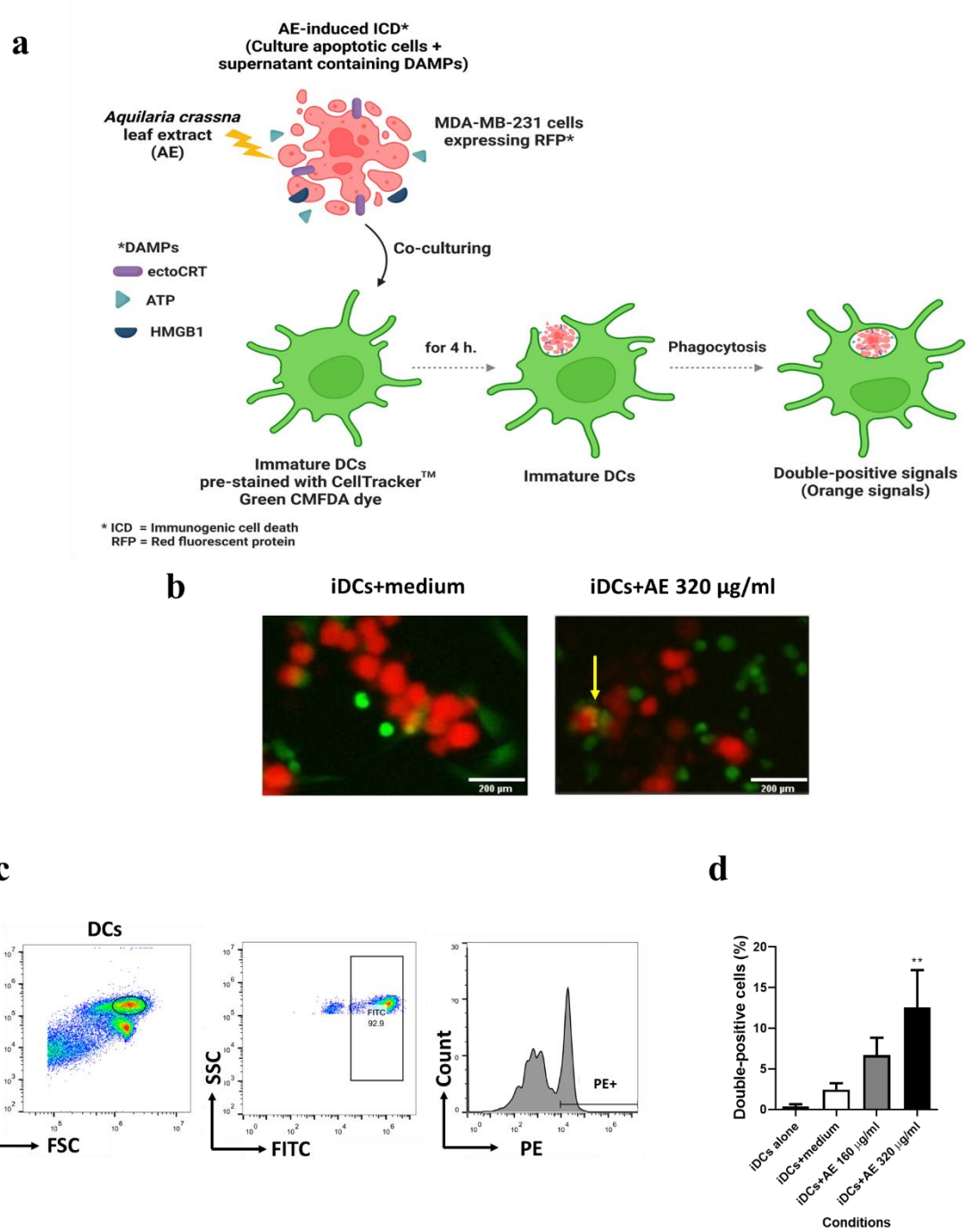

Figure 4 AE-induced ICD enhances dendritic cell (DC) phagocytotic activity. Monocyte-derived immature DCs (iDCs) pre-stained with Cell Tracker™ Green CMFDA, were pulsed with AE-induced ICD generated by treating MDA-MB-231 cells expressing stable red fluorescent protein (RFP) with AE at concentrations of 0, 160 and 320 µg/mL for 48 h. The pre-stained iDCs were then exposed to culture cells and conditioned media of each treatment condition, including untreated (iDCs + medium), AE treatment at 160 µg/mL (iDCs + AE 160 µg/mL), and AE treatment at 320 µg/mL (iDCs + AE 320 µg/mL) for 4 h (a). Phagocytotic activity was assessed by examining double-positive signals from green fluorescent DCs and RFP-expressing MDA-MB-231 cells using fluorescence microscopy and flow cytometry. A representative fluorescence result is illustrated in the iDCs + AE 320 µg/mL condition, indicated by an orange signal with an arrow (b). The gated DC population (positive green fluorescence signal) was selected for further examination of RFP-positive signals (c). The bar graph depicts the percentages of double-positive cells (d). Data represents mean ± SEM of at least 3 independent experiments. ** indicates $p < 0.01$.

Morphological and phenotypic characteristics of DC maturation in iDCs pulsed with AE-induced ICD

In tandem with assessing the phagocytotic activity of DCs, we conducted comprehensive characterizations of morphological and phenotypic maturation to elucidate the augmentation of DC maturation induced by AE-induced ICD. iDCs subjected to AE-induced ICD, underwent morphological scrutiny under a light microscope after an extended pulsing duration of 48 h. Microscopic images unveiled distinctive features in iDC pulsed with AE-induced ICD, particularly at 320 µg/mL, showcasing irregular shapes, significantly enlarged sizes, cell surface ruffles, and the emergence of multiple elongated dendrites (**Figure 5(a6)**). This was in stark contrast to control iDC - iDC treated with medium **(Figure 5(a2))**. Control groups included precursor cells (monocytes) and iDC treated with TNF-α and IFN-γ, serving as controls for DC differentiation and positive control of DC maturation, respectively (**Figures 5(a1)** and **5(a3)**).

To affirm the impact of AE-induced ICD on DC maturation, the expression of co-stimulatory surface molecules, namely CD40, HLA-DR, CD80, CD83, and CD86, was examined in terms of both the percentages of positive-cells and relative MFI analysis. The results demonstrated an escalating trend in the relative MFI of CD86 expression with AE-induced ICD at both 160 and 320 µg/mL. However, statistical significance was attained only at 320 µg/mL when compared to iDC treated with medium (0 µg/mL), with a relative MFI of 1.38 ± 0.10 and 1.00 ± 1.00, respectively, as illustrated in **Figure 5(d)**. Furthermore, the percentages of positive cells of CD80, CD83, HLA-DR, and the relative MFIs of CD80 and CD83 displayed a similar increasing trend, with significant difference observed at 320 µg/mL of AE induction (**Figures 5(b)** - **5(f)**). In summary, AE exerts a potent influence on enhancing DC maturation and activation, as substantiated by both morphological and phenotypic characterizations, particularly through a pronounced increase in CD86 expression.

a

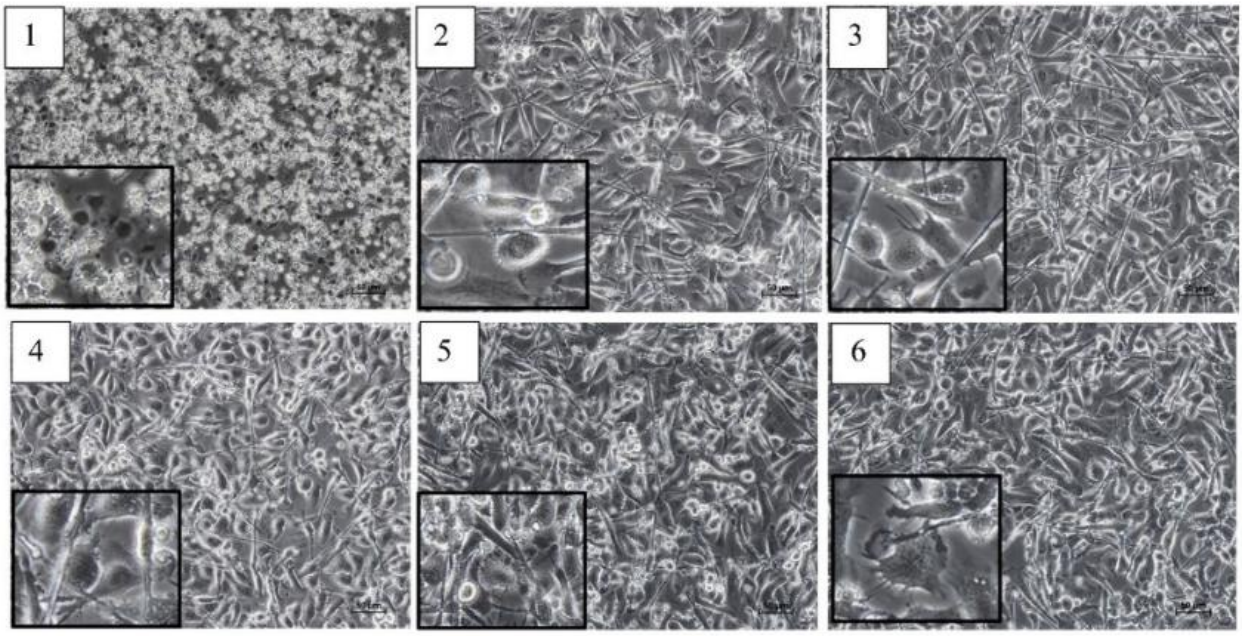

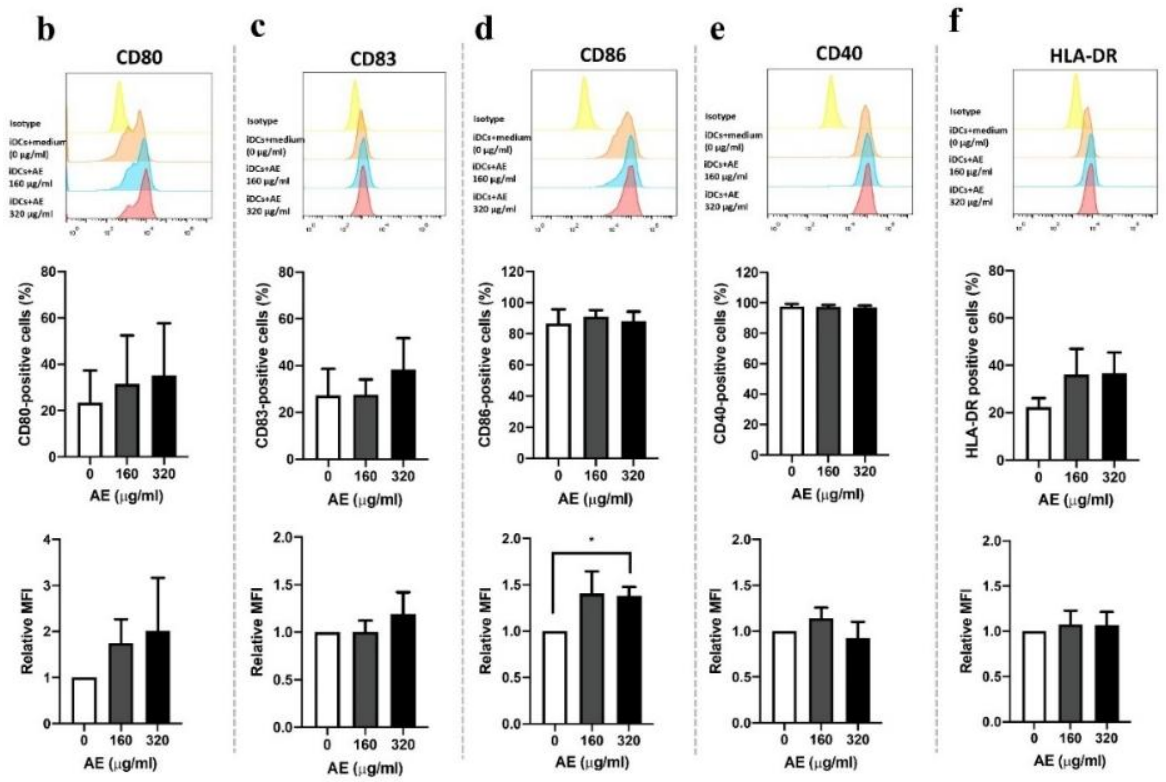

Figure 5 AE-induced ICD enhances expression of co-stimulatory surface molecules on DCs. Monocyte-derived immature DCs (iDCs) were pulsed with AE-induced ICD conditions, including cell lysates and concentrated conditioned media from AE-treated MDA-MB-231 cells at concentrations of 0, 160, and 320 μg/mL for 48 h, alongside a positive control of DC maturation for 2 days. Morphological and phenotypic maturation characteristics were examined using a light microscope at 20× magnification and immunophenotyping. Representative images illustrate cell morphology in various conditions, including monocyte precursor cells (a1), iDCs + AIM-V medium (a2), iDCs + AIM-V medium supplemeted with TNFα and IFN-γ as a positive control for conventional DC maturation (a3), iDCs + 0 μg/mL (a4), iDCs + AE 160 μg/mL (a5), and iDCs + AE 320 μg/mL (a6). The b-f represent the surface expression of CD80, CD83, CD86, CD40, and HLA-DR on iDCs in conditions of iDCs + 0 μg/mL, iDCs + AE 160 μg/mL, and iDCs + AE 320 μg/mL measured by immunophenotyping using specific antibodies for each molecule and analyzed using flow cytometry. Representative histograms (b-f; upper) and bar graphs illustrating the percentages of positive cells (b-f; center), and relative mean fluorescence intensity (MFI) are presented in the bottom sections of b-f, respectively. The relative MFI was calculated in comparison to iDCs + 0 μg/mL condition. Data are presented as mean ± SEM from 3 independent donors. *indicates $p < 0.05$ (unpaired Student's t-test, control and 320 μg/mL of AE).

Discussion

Triple-negative breast cancer (TNBC) stands out as the most aggressive form with the bleakest prognosis among all types of BC, constituting approximately 15% - 20% of all BC cases. Characterized by the absence of estrogen (ER), progesterone (PR), and human epidermal growth factor-2 receptor (HER-2) expression, TNBC presents a unique challenge as it remains unresponsive to hormonal and HER-2-targeted therapies [20,21]. Presently, the mainstay treatment for BC, including TNBC, encompass chemotherapy and 2 immunotherapeutic modalities: Vaccines and immune checkpoint inhibitors (ICI). Nevertheless, the suboptimal response rates and the emergence of serious adverse effects associated with these interventions underscore the imperative need for the innovation and development of novel, more promising, and highly effective strategies for TNBC treatment [22,23].

Aquilaria species are renowned for their substantial economic and medicinal value. Beyond the coveted agarwood oil, various parts of these plants, such as the leaves, have garnered attention for their medicinal

and anti-tumor properties [4,8]. Among the *Aquilaria* species, *Aquilaria crassna* (*A. crassna*) Pierre ex Lecomte stands out prominently. The leaf extract of *A. crassna* Pierre ex Lecomte (AE) demonstrates a myriad of bioactivities, including its capability to induce apoptosis in BC models [1,5,6]. Furthermore, mangiferin, a bioactive compound present in *A. crassna,* has been previously acknowledged for its anti-cancer attributes and immunostimulatory effects [17,18]. However, there is currently a lack of evidence demonstrating the anti-tumor activities of AE or its potential to induce immunogenic cell death (ICD), a process with the capacity to activate the anti-tumor effects of dendritic cells (DCs).

In this study, we elucidate the role of AE in inducing apoptotic and ICD, thereby augmenting the anti-tumor activities of DCs in TNBC model. A prior study by Jang *et al*. [12] documented the anti-tumor effect of *A. crassna* Pierre ex Lecomte, demonstrating apoptosis induction and angiogenesis inhibition in MDA-MB-231 and MCF-7 cells through agarwood extract utilization. In our investigation, bioactive components of AE were identified using validated HPLC. The analysis confirmed the presence of all 4 main bioactive components in our prepared AE, including iriflophenone 3,5-*C*-*β*-D-diglucoside (4.80 ± 0.09 %w/w), iriflophenone 3-*C*-*β*-D-glucoside (1.04 ± 0.01 %w/w), mangiferin (4.54 ± 0.33 %w/w), and genkwanin 5-*O*-*β*-primevoside (0.18 ± 0.02 %w/w). To standardize the extract, AE was monitored for quality by regulating the quantities of the 4 principal bioactive constituents, compound 1 - 4. The controlling amounts must be no less than 3%, 1%, 4% and 0.05%, respectively. Those regulating quantities were apprehensive regarding their capacity for biological activities, as determined by the research group that reported other biological activities utilizing AE produced from the same technique [7,24].

These constituents, recognized for their antioxidant, antiglycation, and anti-inflammatory, and vasodilator properties, align with prior reports [6,7]. Remarkably, mangiferin, a well-known compound for its anti-tumor and immunomodulatory effects, emerged as the second most abundant component in AE (**Table 1**). Furthermore, the stability of compounds 1 - 3 in both powdered form and aqueous solution was established in a previous study [19]. Predictions of the shelf life ($t_{90\%}$) at 25 °C for the powdered form of compounds 1 - 3 in AE, using Arrhenius plot, revealed a shelf life of 989 days, 248 days, and unpredictability, respectively. In contrast, the shelf life of their solution form at 25 °C was shorter, at 189, 13 and 75 days, respectively. This information underscores the stability of compounds 1 - 3 in aqueous solutions, ensuring their viability for use in cell cultures for 48 h. This duration is deemed sufficient for inducing ICD or DAMPs expression in our studies.

AE displayed a dose-dependent anti-tumor effect, evident in the reduction of MDA-MB 231 cell viability across the 0 - 640 µg/mL range (**Figure 2(a)**). The IC_{50} values for AE treatment at 24 and 48 h were found to be 148.3 and 91.93 µg/mL, respectively. It is noteworthy that Jang *et al.* [12] observed anti-tumor activity against MDA-MB 231 cells, although they did not report the corresponding IC_{50} value. In a separate study, Abbas *et al.* [25] investigated the cytotoxic impact of *Aquilaria subintegra* (*A. subintegra*) leaf extract on MCF-7 cells, revealing a 4.52% cell viability at 100 µg/mL of *A. subintegra* after 24 h, determined through cell counting procedure. Importantly, our study is the inaugural report illustrating the cytotoxicity of AE on the TNBC model. The observed disparities in cytotoxicity induction between their study and ours may be attributed to variances in *Aquilaria* species and cell types. Furthermore, our study also revealed that AE is less toxic on non-tumorigenic cells than the tumorigenic cells. At the maximal dose of 640 µg/mL, AE demonstrated the highest toxicity on TNBC, exhibiting less harm to MCF-10A cells compared to MDA-MB-231 cells (**Figures 2(a)** and **2(b)**). This result is supported by the study in normal cells, rat isolated smooth muscle cells. They demonstrated no cytotoxicity in normal smooth muscle cells in a concentration of 1,000 µg/mL of AE [6].

We further elucidated the role of AE as an inducer of ICD, substantiated by its capacity to prompt apoptosis in MDA-MB-231 cells. Notably, a pronounced increase in apoptosis was evident, particularly at the 48-hour time point, with apoptosis levels reaching 27.42 ± 5.30% and 32.07 ± 3.10% at concentrations of 160 and 320 µg/mL, respectively (**Figures 2(e)** and **2(f)**). In the context of this apoptotic induction, AE resulted in a substantial rise in secreted ATP (**Figure 3(h)**) and elevated levels of HMGB1 (**Figures 3(i) - 3(k)**).

Moreover, a significant relative mean fluorescence intensity (MFI) of ectoCRT was detected as early as 12 h into the treatment (**Figure 3(g)**). These findings align with prior studies, both *in vitro* and *in vivo*, investigating the impact of various chemotherapeutic agents and natural products. For example, Quan *et al.* [26] explored the use of ethanol extract of *Cordyceps militaris* in MDA-MB-231 cells, noting a 40% induction of apoptosis and a substantial increase in ectoCRT expression within a 6 - 72 h timeframe. Similarly, an examination of cholangiocarcinoma apoptosis cells treated with Honokiol isolated from *Magnolia officinalis* demonstrated HMGB1 expression between 24 and 48 h [27]. Additionally, low doses of gemcitabine significantly increased ectoCRT and HMGB1 expression levels after 24 h of the treatment in the Lewis lung carcinoma (LLC) cell line [28]. In addition to those inducers, the 3 DAMPs markers inducted by AE were accorded to other known inducers such as anthracyclines, γ-irradiation, and oncolytic viruses [29-31].

Our findings unequivocally establish that AE possesses the capacity to induce key DAMPs expression, akin to standard chemotherapeutic drugs or established ICD inducers. This observation suggests that the ICD induced by AE in our study holds promise for instigating an anti-tumor response in BC. ICD has emerged as a highly promising strategy for triggering adaptive immune responses against tumors [32]. The heightened immunogenicity resulting from ICD aligns with the criteria for an endogenous vaccine or DC-based vaccine, proven effective in activating DCs and enhancing antitumor immunity [33]. Moreover, ICD-based cancer monotherapy has demonstrated efficacy in treating metastatic breast cancer and retroperitoneal sarcoma. Some such therapies are currently in preclinical or clinical development, often as part of combination therapy with conventional chemotherapeutic ICD inducers and emerging immune checkpoint inhibitor (ICI) like anti-PD1 and CTLA-4, spanning various cancer types [34-36]. ICD is linked to the activation of the intracellular stress response, either indirectly (type I inducer) or directly (type II inducer), acting on the endoplasmic reticulum (ER) and ultimately culminating in cell death. It is well-established that ER stress, activated by reactive oxygen species (ROS), plays a significant role in ICD [30]. The expression of ectoCRT is essential and involves the unfolded protein response (UPR) via protein kinase RNA-like ER kinase (PERK) and eukaryotic transcription initiation factor 2 (eIF2α) [37]. Simultaneously, the release of ATP into the extracellular space during ICD occurs in the late stage of apoptosis and is associated with autophagic induction [29]. In contrast to ectoCRT and ATP, HMGB1 is passively released into the extracellular space during the late apoptotic/necrotic stage of ICD, when both the nuclear and plasma membranes have been permeabilized [38].

Regrettably, our study did not present data on the underlying mechanism of ICD induced by AE. Drawing on the evidence from other ICD inducers, the majority of them caused ICD by engaging with ER stress, ROS production, and autophagic cell death, implying that AE may induce ICD similarity to established ICD inducers [34,39,40]. For instance, mangiferin has been reported to enhance autophagy in cardiomyocytes and induce autophagy and endogenous ROS production in pancreatic cancer cells [41,42]. Given the mechanism of mangiferin in inducing ROS production, we hypothesized that mangiferin may act as an ICD inducer. Further investigation is required to validate the effects of mangiferin and its underlying mechanism, together with the other 3 bioactive components (compounds 1 - 4), in triggering ICD in BC model. DCs stand out as the most potent professional antigen-presenting cells (APCs) bridging innate and adaptive immune responses against tumors by activating CD8+ and CD4+ T cells [43]. Various cancers, including head and neck squamous cell carcinoma (HNSCC), renal and prostate cancer, and BC, have been associated with decreased numbers of mature DCs, reduced capacity to stimulate T cell proliferation, and spontaneous apoptosis [44-46]. Hence, it is imperative to develop strategic approaches aimed at inducing or augmenting effective DC functions. Our study on AE-induced ICD uncovered the ability to enhance DC maturation, evidenced by an increased phagocytotic ability of immature DCs (iDCs) 4 h after pulsing with AE-induced ICD (**Figure 4(d)**). Furthermore, a morphological maturation of pulsed DCs was observed, transitioning from round and smooth-surfaced iDCs to irregularly shaped cells with a significantly larger size, and ruffles on the cell surface with multiple and longer dendrites. This morphological transformation aligns with the typical characteristics of mature DCs [47]. In addition to morphological

maturation, AE-induced ICD also led to phenotypic maturation of DCs, marked by a significant increase in the expression of CD86, and a trend toward increased expression of other co-stimulatory molecules necessary for T cell activation, such as CD80 and CD83, and HLA-DR. The heightened phagocytotic activity and increased expression of CD86 and CD80 in iDCs pulsed with AE-induced ICD are consistent with findings from a study by Turubanova *et al.* [48], where ICD induced by photosensitizers (photosens and photodithazine) in murine glioma GL261 and fibrosarcoma MCA205 cells resulted in the expression of ectoCRT, secreted ATP and secreted HMGB1, leading to increased phagocytosis of bone-marrow-derived dendritic cells (BMDCs). Another study by Donnelly *et al.* [49] found that secreted HMGB1 induced by the measles virus could induce DC maturation, as evidenced by a significant increase in CD86 and CD80 expression. Hence, it is probable that AE-induced ICD in cancer cells results in heightened maturation of DCs, accompanied by phenotypic changes, activated functions, and elevated expression of additional co-stimulatory molecules. Consequently, this activation is anticipated to enhance the anti-tumor functions of T cells. While our findings may indicate that AE induces ICD and enhances the phagocytosis and maturation of dendritic cells (DCs), further research is required to elucidate AE's role as an immunomodulator in promoting effective cancer cell eradication. Specifically, it is essential to demonstrate that AE-mediated DC maturation subsequently activates T cells, increases T cell infiltration, and ultimately facilitates the efficient destruction of cancer cells, both *in vitro* and *in vivo* as indicated by Quan *et al.* [26]; Jiraviriyakul *et al.* [27]; Zhao *et al.* [50]. We hypothesize that AE-mediated DC maturation may trigger all the described processes, given our findings identified all the earliest stages of ICD-induced immune responses consistent with those studies.

Conclusions

This study is pioneering in revealing the role of AE in inducing ICD, thereby enhancing the anti-tumor function of DCs. AE accomplishes this beneficial activity by instigating apoptotic cell death and significantly elevating the levels of ectoCRT, secreted ATP, and HMGB1 - key indicators of ICD. The resultant AE-induced ICD leads to heightened phagocytotic activity and a marked increase in the expression of CD86, CD80, CD83, and HLA-DR, all indicative of DC maturation. These findings provide fresh insights into the anti-tumor activity and immune-activating effect of AE, particularly concerning DC activation in a TNBC model, complementing the previously documented medicinal activities of AE. Moreover, given the traditionally ensured safety of *A. crassna* leaves through their use in herbal remedies, tea, soup, and other edible products, the study suggests the potential development of AE as a dietary complementary or alternative treatment for anti-tumor purposes in the future. However, to comprehensively understand its efficacy, further studies are essential, particularly in investigating T cell activation and enhancement of cancer cell killing, along with validation in *in vivo* models.

Ethical approval

The protocols for this study received approval from the Naresuan University Institutional Review Board (NUIRB No. P1-0155/2564).

Acknowledgements

This study received financial supported from the Center of Excellence on Medical Biotechnology (CEMB; Grant No. CB-61-006-04), Mahidol University, Thailand. Additionally, Aussara Panya received funding from Chiang Mai University, Thailand.

The authors express gratitude for the technical support provided by the Division of Molecular Medicine, Research Department, Faculty of Medicine Siriraj Hospital, Mahidol University, Bangkok. Additionally, appreciation is extended to the Department of Anatomy, Faculty of Medical Science, Naresuan University. Aussara Panya acknowledges support from Chiang Mai University.

Declaration of generative AI in scientific writing

During the preparation of this work the authors used Paraphrasing Tool (QuillBot) in order to improving clarity and language quality. All scientific content, interpretation, and conclusions were developed independently by the authors. After using this tool/service, the authors reviewed and edited the content as needed and takes full responsibility for the content of the publication.

CRediT author statement

Pinyada Pho-on: Investigation, Formal analysis, Validation, Writing - Original draft preparation. **Sangkab Sudsaward:** Writing-Original draft preparation, Writing -review & editing, Formal analysis, Validation. **Piriya Luangwattananun:** Methodology, Investigation, Validation, Writing - review & editing. **Aussara Panya:** Methodology, Validation, Writing -review & editing. **Chutamas Thepmalee:** Methodology, Validation, Writing -review & editing. **Mutita Junking:** Methodology, Investigation, Resources, Writing -review & editing. **Eakkaluk Wongwad:** Resources, Writing -review & editing. **Kornkanok Ingkaninan:** Resources, Writing - review & editing. **Pattareeya Sereesantiwong:** Formal analysis. **Warintorn Wongho:** Formal analysis. **Pathai Yenchitsomanas:** Conceptualization, Supervision, Resources, Writing -review & editing. **Sasiprapa Khunchai:** Conceptualization, Methodology, Investigation, Validation, Resources, Project administration, Writing - Original Draft, Writing - Review & Editing, Funding acquisition.

References

[1] S Kamonwannasit, N Nantapong, P Kumkrai, P Luecha, S Kupittayanant and N Chudapongse. Antibacterial activity of *Aquilaria crassna* leaf extract against Staphylococcus epidermidis by disruption of cell wall. *Annals of Clinical Microbiology and Antimicrobials* 2013; **12(1)**, 20.

[2] H Okugawa, R Ueda, K Matsumoto, K Kawanishi and A Kato. Effects of agarwood extracts on the central nervous system in mice. *Planta Medica* 1993; **59(1)**, 32-36.

[3] H Okugawa, R Ueda, K Matsumoto, K Kawanishi and A Kato. Effect of jinkoh-eremol and agarospirol from agarwood on the central nervous system in mice. *Planta Medica* 1996; **62(1)**, 2-6.

[4] G Ray, W Leelamanit, P Sithisarn and W Jiratchariyakul. Anti-oxidative compounds from *Aquilaria crassna* leaf. *Mahidol University Journal of Pharmaceutical Sciences* 2014; **41**, 54-58.

[5] N Pattarachotanant, P Rangsinth, W Warayanon, GPH Leung, S Chuchawankul, A Prasansuklab and T Tencomnao. Protective effect of aquilaria crassna leaf extract against benzo[a]pyrene-induced toxicity in neuronal cells and *Caenorhabditis elegans:* Possible active constituent includes clionasterol. *Nutrients* 2023; **15(18)**, 3985.

[6] S Wisutthathum, N Kamkaew, A Inchan, U Chatturong, TU Paracha, K Ingkaninan, E Wongwad and K Chootip. Extract of *Aquilaria crassna* leaves and mangiferin are vasodilators while showing no cytotoxicity. *Journal of Traditional and Complementary Medicine* 2019; **9(4)**, 237-242.

[7] E Wongwad, C Pingyod, T Saesong, N Waranuch, W Wisuitiprot, B Sritularak, P Temkitthawon and K Ingkaninan. Assessment of the bioactive components, antioxidant, antiglycation and anti-inflammatory properties of *Aquilaria crassna* pierre ex lecomte leaves. *Industrial Crops and Products.* 2019; **138**, 111448.

[8] YZ Hashim, A Phirdaous and A Azura. Screening of anticancer activity from agarwood essential oil. *Pharmacognosy Research* 2014; **6(3)**, 191-194.

[9] W Putalun, G Yusakul, P Saensom, B Sritularak and H Tanaka. Determination of iriflophenone 3-C-beta-d-glucoside from Aquilaria spp. by an indirect competitive enzyme-linked immunosorbent assay using a specific polyclonal antibody. *Journal of Food Science* 2013; **78(9)**, C1363-C1367.

[10] SS Dahham, YM Tabana, LEA Hassan, MBK Ahamed, ASA Majid and AMSA Majid. *In vitro* antimetastatic activity of Agarwood (*Aquilaria crassna*) essential oils against pancreatic cancer cells. *Alexandria Journal of Medicine* 2016; **52(2)**, 141-150.

[11] SS Dahham, YM Tabana, MA Iqbal, MBK Ahamed, MO Ezzat, ASA Majid and AMSA Majid. The anticancer, antioxidant and antimicrobial properties of the sesquiterpene beta-caryophyllene from the essential oil of aquilaria crassna. *Molecules* 2015; **20(7)**, 11808-11829.

[12] HM Jang, JH Lee, JH Kim, G Park and JH Jeon. *In vitro* anticancer effect of Aquilaria crassna extract on human mammary gland cancer cells. *International journal of Biosciences* 2020; **16(4)**, 187-192.

[13] L Galluzzi, E Guilbaud, D Schmidt, G Kroemer and FM Marincola. Targeting immunogenic cell

stress and death for cancer therapy. *Nature Reviews Drug Discovery* 2024; **23(6)**, 445-460.

[14] N Nagarsheth, MS Wicha and W Zou. Chemokines in the cancer microenvironment and their relevance in cancer immunotherapy. *Nature Reviews Immunology* 2017; **17(9)**, 559-572.

[15] L Galluzzi, I Vitale, S Warren, S Adjemian, P Agostinis, AB Martinez, TA Chan, G Coukos, S Demaria, E Deutsch, D Draganov, RL Edelson, SC Formenti, J Fucikova, L Gabriele, US Gaipl, SR Gameiro, AD Garg, E Golden, …, KJ Harrington. Consensus guidelines for the definition, detection and interpretation of immunogenic cell death. *The Journal for ImmunoTherapy of Cancer* 2020; **8(1)**, e000337.

[16] DR Green, T Ferguson, L Zitvogel and G Kroemer. Immunogenic and tolerogenic cell death. *Nature Reviews Immunology* 2009; **9(5)**, 353-363.

[17] SN Morozkina, THN Vu, YE Generalova, PP Snetkov and MV Uspenskaya. Mangiferin as new potential anti-cancer agent and mangiferin-integrated polymer systems-a novel research direction. *Biomolecules* 2021; **11(1)**, 79.

[18] S Muruganandan, J Lal and PK Gupta. Immunotherapeutic effects of mangiferin mediated by the inhibition of oxidative stress to activated lymphocytes, neutrophils and macrophages. *Toxicology* 2005; **215(1-2)**, 57-68.

[19] E Wongwad, K Ingkaninan, W Wisuitiprot, B Sritularak and N Waranuch. Thermal degradation kinetics and pH-Rate profiles of iriflophenone 3,5-C-beta-d-diglucoside, iriflophenone 3-C-beta-d-glucoside and mangiferin in aquilaria crassna leaf extract. *Molecules* 2020; **25(21)**, 4898.

[20] S Hurvitz and M Mead. Triple-negative breast cancer: Advancements in characterization and treatment approach. *Current Opinion in Obstetrics and Gynecology* 2016; **28(1)**, 59-69.

[21] BD Lehmann, JA Bauer, X Chen, ME Sanders, AB Chakravarthy, Y Shyr and JA Pietenpol. Identification of human triple-negative breast cancer subtypes and preclinical models for selection of targeted therapies. *Journal of Clinical Investigation* 2011; **121(7)**, 2750-2767.

[22] LB Kennedy and AKS Salama. A review of cancer immunotherapy toxicity. *CA: A Cancer Journal for Clinicians* 2020; **70(2)**, 86-104.

[23] HL McArthur and DB Page. Immunotherapy for the treatment of breast cancer: checkpoint blockade, cancer vaccines, and future directions in combination immunotherapy. *Clinical Advances in Hematology & Oncology* 2016; **14(11)**, 922-933.

[24] C Supasuteekul, S Tadtong, W Putalun, H Tanaka, K Likhitwitayawuid, P Tengamnuay and B Sritularak. Neuritogenic and neuroprotective constituents from Aquilaria crassna leaves. *Journal of Food Biochemistry* 2017; **41(3)**, e12365.

[25] P Abbas, Y Hashim and HM Salleh. Uninfected agarwood branch extract possess cytotoxic and inhibitory effects on MCF-7 breast cancer cells. *Journal of Research in Pharmacy* 2019; **23(1)**, 120-129.

[26] X Quan, BS Kwak, JY Lee, JH Park, A Lee, TH Kim and SG Park. *Cordyceps militaris* induces immunogenic cell death and enhances antitumor immunogenic response in breast cancer. *Evidence-Based Complementary and Alternative Medicine* 2020; **2020(6)**, 1-11.

[27] A Jiraviriyakul, W Songjang, P Kaewthet, P Tanawatkitichai, P Bayan and S Pongcharoen. Honokiol-enhanced cytotoxic T lymphocyte activity against cholangiocarcinoma cells mediated by dendritic cells pulsed with damage-associated molecular patterns. *World Journal of Gastroenterology* 2019; **25(29)**, 3941-3955.

[28] X Zhang, D Wang, Z Li, D Jiao, L Jin, J Cong, X Zheng and L Xu. Low-dose gemcitabine treatment enhances immunogenicity and natural killer cell-driven tumor immunity in lung cancer. *Frontiers in Immunology* 2020; **11**, 331.

[29] L Galluzzi, A Buqué, O Kepp, L Zitvogel and G Kroemer. Immunogenic cell death in cancer and infectious disease. *Nature Reviews Immunology* 2017; **17(2)**, 97-111.

[30] DV Krysko, AD Garg, A Kaczmarek, O Krysko, P Agostinis and P Vandenabeele. Immunogenic cell death and DAMPs in cancer therapy. *Nature Reviews Cancer* 2012; **12(12)**, 860-875.

[31] J Zhang, J Chen and K Lin. Immunogenic cell death-based oncolytic virus therapy: A sharp sword of tumor immunotherapy. *European Journal of Pharmacology.* 2024; **981**, 176913.

[32] MJ Smyth, SF Ngiow, A Ribas and MWL Teng. Combination cancer immunotherapies tailored to the tumour microenvironment. *Nature Reviews Clinical Oncology* 2016; **13(3)**, 143-158.

[33] MJ Lamberti, A Nigro, FM Mentucci, NBR Vittar, V Casolaro and JD Col. Dendritic cells and immunogenic cancer cell death: A combination for improving antitumor immunity. *Pharmaceutics* 2020; **12(3)**, 256.

[34] Z Asadzadeh, E Safarzadeh, S Safaei, A Baradaran, A Mohammadi, K Hajiasgharzadeh, A Derakhshani, A Argentiero, N Silvestris and B Baradaran. Current approaches for combination therapy of cancer: The role of immunogenic cell death. *Cancers* 2020; **12(4)**, 1047.

[35] A Azami, N Suzuki, Y Azami, I Seto, A Sato, Y Takano, T Abe, Y Teranishi, K Tachibanan and T Ohtake. Abscopal effect following radiation monotherapy in breast cancer: A case report. *Molecular and Clinical Oncology* 2018; **9(3)**, 283-286.

[36] J Banchereau and RM Steinman. Dendritic cells and the control of immunity. *Nature* 1998; **392(6673)**, 245-252.

[37] O Kepp, M Semeraro, JMBS Pedro, N Bloy, A Buqué, X Huang, H Zhou, L Senovilla, G Kroemer and L Galluzzi. EIF2alpha phosphorylation as a biomarker of immunogenic cell death. *Seminars in Cancer Biology* 2015; **33**, 86-92.

[38] IE Dumitriu, P Baruah, B Valentinis, RE Voll, M Herrmann, PP Nawroth, B Arnold, ME Bianchi, AA Manfredi and P Rovere-Querini. Release of high mobility group box 1 by dendritic cells controls T cell activation via the receptor for advanced glycation end products. *The Journal of Immunology* 2005; **174(12)**, 7506-7515.

[39] H Inoue and K Tani. Multimodal immunogenic cancer cell death as a consequence of anticancer cytotoxic treatments. *Cell Death & Differentiation* 2014; **21(1)**, 39-49.

[40] J Zhou, G Wang, Y Chen, H Wang, Y Hua and Z Cai. Immunogenic cell death in cancer therapy: Present and emerging inducers. *Journal of Cellular and Molecular Medicine* 2019; **23(8)**, 4854-4865.

[41] J Hou, D Zheng, W Xiao, D Li, J Ma and Y Hu. Mangiferin enhanced autophagy via inhibiting mTORC1 pathway to prevent high glucose-induced cardiomyocyte injury. *Frontiers in Pharmacology* 2018; **9**, 383.

[42] L Yu, M Chen, R Zhang and Z Jin. Inhibition of cancer cell growth in gemcitabine-resistant pancreatic carcinoma by mangiferin phytochemical involves induction of autophagy, endogenous ROS production, cell cycle disruption, mitochondrial mediated apoptosis and suppression of cancer cell migration and invasion. *Journal of Balkan Union of Oncology* 2019; **24(4)**, 1581-1586.

[43] H Harizi. Reciprocal crosstalk between dendritic cells and natural killer cells under the effects of PGE2 in immunity and immunopathology. *Cellular & Molecular Immunology* 2013; **10(3)**, 213-221.

[44] TK Hoffmann, J Müller-Berghaus, RL Ferris, JT Johnson, WJ Storkus and TL Whiteside. Alterations in the frequency of dendritic cell subsets in the peripheral circulation of patients with squamous cell carcinomas of the head and neck. *Clinical Cancer Research* 2002; **8(6)**, 1787-1793.

[45] C Lenahan and D Avigan. Dendritic cell defects in patients with cancer: Mechanisms and significance. *Breast Cancer Research* 2006; **8(1)**, 101.

[46] AJ Troy, KL Summers, PJ Davidson, CH Atkinson and DN Hart. Minimal recruitment and activation of dendritic cells within renal cell carcinoma. *Clinical Cancer Research* 1998; **4(3)**, 585-593.

[47] MK Kim and J Kim. Properties of immature and mature dendritic cells: Phenotype, morphology, phagocytosis, and migration. *RSC Advances* 2019; **9(20)**, 11230-1138.

[48] VD Turubanova, IV Balalaeva, TA Mishchenko, E Catanzaro, R Alzeibak, NN Peskova, I Efimova, C Bachert, EV Mitroshina, O Krysko, MV Vedunova and DV Krysko. Immunogenic cell death induced by a new photodynamic therapy based on photosens and photodithazine. *Journal for ImmunoTherapy of Cancer* 2019; **7(1)**, 350.

[49] OG Donnelly, F Errington-Mais, L Steele, E Hadac, V Jennings, K Scott, H Peach, RM Phillips, J Bond, H Pandha, K Harrington, R Vile, S Russell, P Selby and AA Melcher. Measles virus causes

immunogenic cell death in human melanoma. *Gene Therapy volume* 2013; **20(1)**, 7-15.

[50] X Zhao, K Yang, R Zhao, T Ji, X Wang, X Yang, Y Zhang, K Cheng, S Liu, J Hao, H Ren, KW Leong and G Nie. Inducing enhanced immunogenic cell death with nanocarrier-based drug delivery systems for pancreatic cancer therapy. *Biomaterials* 2016; **102**, 187-197.